Journal of Solid State Chemistry 183 (2010) 1127–1132

Contents lists available at ScienceDirect

Journal of Solid State Chemistry

journal homepage: www.elsevier.com/locate/jssc

Cerium luminescence in nd^0 perovskites

A.A. Setlur [a,*], U. Happek [b]

[a] GE Global Research Center, 1 Research Circle, Niskayuna, NY 12309, USA
[b] Department of Physics and Astronomy, University of Georgia, Athens, GA 30602, USA

ARTICLE INFO

Article history:
Received 14 December 2009
Accepted 17 March 2010
Available online 20 March 2010

Keywords:
Perovskites
Ce^{3+}
Luminescence

ABSTRACT

The luminescence of Ce^{3+} in perovskite (ABO_3) hosts with nd^0 B-site cations, specifically Ca(Hf,Zr)O_3 and (La,Gd)ScO_3, is investigated in this report. The energy position of the Ce^{3+} excitation and emission bands in these perovskites is compared to those of typical Al^{3+} perovskites; we find a Ce^{3+} $5d^1$ centroid shift and Stokes shift that are larger versus the corresponding values for the Al^{3+} perovskites. It is also shown that Ce^{3+} luminescence quenching is due to Ce^{3+} photoionization. The comparison between these perovskites shows reasonable correlations between Ce^{3+} luminescence quenching, the energy position of the Ce^{3+} $5d^1$ excited state with respect to the host conduction band, and the host composition.

1. Introduction

The relative simplicity of the Ce^{3+} energy levels has led to phenomenological models for the position of the $5d^1$ centroid and the crystal field splitting of the $5d^1$ levels [1,2]. There are also empirical rules to understand the parameters for Ce^{3+} photoionization quenching, starting with a minimum host bandgap for efficient Ce^{3+} luminescence in oxides [3] with further work towards understanding the position of the Ce^{3+} $4f^1$ ground state within the host lattice bandgap [4]. This work to quantify and understand Ce^{3+} luminescence has practical implications since Ce^{3+} luminescence is used in many efficient phosphors and scintillators, and additional progress towards the relationship between host composition and Ce^{3+} luminescence could lead to insight for the design of these materials.

One approach to understand host lattice effects on luminescence is to analyze the luminescence properties versus composition for a set of isostructural hosts [5]. For Ce^{3+} luminescence, the ABO_3 perovskites could be instructive for comparisons with compositional variations of the larger A cation and the smaller, octahedral B cation (with a caveat for distortions in the octahedral arrays for different A/B combinations). Prior work in Al^{3+} perovskites has studied the effect of composition on the energy position of the Ce^{3+} $4f^1 \rightarrow 5d^1$ transitions [1] as well as photoionization quenching [6,7]. We expand upon this prior work by studying Ce^{3+} luminescence in perovskite hosts that have B-site cations with nd^0 configurations, specifically $LaScO_3$, $GdScO_3$, $CaHfO_3$, and $CaZrO_3$. Using the relationship between the average cation electronegativity and A–O bonding in perovskites and the Ce^{3+} $5d^1$ centroid shift and crystal field splitting [1,2], it is possible to correlate the perovskite composition to the energy position of the lowest Ce^{3+} $4f^1 \rightarrow 5d^1$ transition. In regard to the Ce^{3+} luminescence quenching, while the absorption edge of these perovskites are at relatively low energies (<5.9 eV) [8,9], there are significant differences in the thermal quenching of the $5d^1 \rightarrow 4f^1$ Ce^{3+} luminescence. A Born–Haber method [10] is used to analyze the photoionization thresholds and gives a qualitative correlation between the Ce^{3+} luminescence efficiency and perovskite composition. Therefore, we demonstrate systematic compositional trends in these perovskites for both the energy position of the lowest Ce^{3+} $5d^1$ level and photoionization quenching of Ce^{3+} luminescence.

2. Experimental procedure

Standard solid-state synthesis methods using high purity $CaCO_3$, La_2O_3, Gd_2O_3, Lu_2O_3, Sc_2O_3, HfO_2, ZrO_2, and CeO_2 were used to make powder samples. Ce^{3+} ions replace the larger A-site cations at nominal levels of 0.1–1%, and for Ca(Hf,Zr)O_3, there is no intentional charge compensation. The compositions reported here are nominal compositions and all samples are single-phase orthorhombic perovskites as determined by powder X-ray diffraction with the exception of $LaScO_3$ that has a trace ($<5\%$) of unreacted La_2O_3. However, La_2O_3:Ce^{3+} does not have any luminescence at liquid He temperatures [3] and should not interfere with the luminescence studies reported here.

Excitation and emission spectra were measured using a Spex Fluoromax 2 spectrofluorometer with a closed cycle He cryostat that has a cold finger attachment. Diffuse reflectance

* Corresponding author. Fax: +1 518 387 6204.
E-mail address: setlur@ge.com (A.A. Setlur).

0022-4596/$ - see front matter © 2010 Elsevier Inc. All rights reserved.
doi:10.1016/j.jssc.2010.03.025

measurements used the same spectrometer with $BaSO_4$ (Kodak) as a reflectance standard. Time resolved measurements from 77 to 450 K used a LED excitation source filtered through a narrow band interference filter (10 nm width) driven by the amplified (Avantec) pulses of an Avtech AVP-C pulse generator. The emission was filtered through a 0.5 m McPherson monochromator and detected with a Hamamatsu R212 PMT detector. The time resolved fluorescence was recorded through a photon counting system consisting of an Ortec 567 time-to-amplitude converter in conjunction with an EG & G pulse height analyzer. The temporal response for this experimental setup was measured at 2 ns. Time resolved measurements above 300 K also used powder pressed into a Al plaque with cartridge heaters, thermocouples, and a Watlow temperature controller and a tripled Nd:YAG laser at 355 nm (JDS Uniphase) coupled into an Edinburgh F900 spectrofluorometer with a Peltier cooled R928-P Hamamatsu photomultiplier tube (PMT) detector. The FWHM of the laser pulse convoluted with the overall system response is ~1 ns. Measurements of the thermoluminescence excitation spectra (TLES) followed previously reported procedures [11].

3. Results and discussion

3.1. Luminescence of $CaHfO_3:Ce^{3+}$ and $CaZrO_3:Ce^{3+}$

The emission and excitation of $CaHfO_3:Ce^{3+}$ are indicative of typical Ce^{3+} luminescence with a doublet emission band consisting that can be fit by two Gaussians separated by ~2000 cm^{-1} with λ_{max}~430 nm (Fig. 1a). The maximum of the excitation band is at ~335 nm (~29 900 cm^{-1}) giving a Stokes shift of ~6700 cm^{-1}. When accounting for the ~12 240 ± 750 cm^{-1} energy difference between the lowest energy Ce^{3+} $4f^1 \rightarrow 5d^1$ and Pr^{3+} $4f^2 \rightarrow 4f^1 5d^1$ transitions [12], the position of the $CaHfO_3:Ce^{3+}$ excitation band reported here is in reasonable correlation with the position of the main Pr^{3+} excitation band in $CaHfO_3$ (~41 700 cm^{-1}) [13]. In addition, the Stokes shift for Ce^{3+} and Pr^{3+} $4f^{N-1}5d^1 \rightarrow 4f^N$ emission is similar (6700 cm^{-1} for Ce^{3+} vs. 7600 cm^{-1} for Pr^{3+}) as expected. The Stokes shift for Ce^{3+} luminescence is also larger in comparison to the Al^{3+} perovskites but is similar to the Stokes shift for $LaLuO_3:Ce^{3+}$ [14] (Table 1), indicating a potential relationship between the B-site cation size and the Ce^{3+} Stokes shift. The energy position of the lowest Ce^{3+} $5d^1$ level in $CaHfO_3$ is lower when compared to the Al^{3+} perovskites (Table 1); this is primarily due to the lower electronegativity of both Hf^{4+} and Ca^{2+} versus Al^{3+} and the trivalent lanthanides [15], respectively. The lower average cation electronegativity increases the O^{2-} anion polarizability and the covalency of the Ce^{3+}–O^{2-} bond (via an inductive effect), leading to a larger Ce^{3+} $5d^1$ centroid shift [2].

In spite of the low energy position of the absorption edge and the relatively large Stokes shift, $CaHfO_3:Ce^{3+}$ has weak thermal quenching at room temperature (Figs. 1b and 2), and initial measurements of the quantum efficiency (λ_{ex}~335 nm) at room temperature is ~30% of a standard $BaMgAl_{10}O_{17}:Eu^{2+}$ blue phosphor, a reasonably high value for unoptimized samples. As the initial decay time of $CaHfO_3:Ce^{3+}$ begins to decrease, the decay profile deviates from a single exponential with an additional weak component that has a decay time of > 30 ns, slower than the radiative decay rate (Fig. 1b). This slower decay component is assigned to an afterglow luminescence that occurs after charge carriers are created, trapped at defects, and slowly detrapped from those defects. The correlation between the

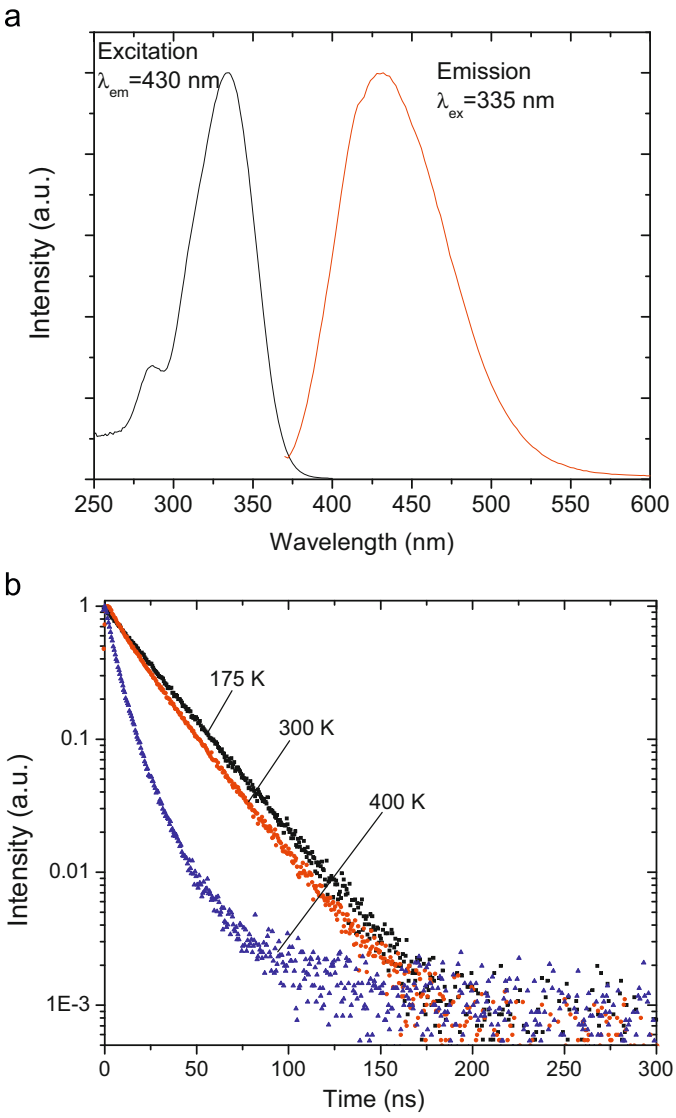

Fig. 1. (a) Emission (λ_{ex}=335 nm) and excitation spectra of (λ_{em}=430 nm) of $Ca_{0.99}Ce_{0.01}HfO_3$ at ~10 K and (b) Decay profiles (λ_{ex}=320 nm, λ_{em}=440 nm) versus temperature for $Ca_{0.999}Ce_{0.001}HfO_3$. The background has been subtracted from these decay profiles.

Table 1
Emission and excitation peaks for Ce^{3+}-doped perovskites.

Host	Excitation (cm^{-1})	Emission (cm^{-1})	Stokes shift (cm^{-1})	Reference
$CaHfO_3$	29 900	23 200	6700	This work
$LaScO_3$	30 950	23 300	7700	This work
$GdScO_3$	28 650	23 300	5350	This work
$YAlO_3$	33 000	28 500	4500	[26]
$GdAlO_3$	32 500	29 590	2900	[27]
$LaAlO_3$	31 750	No emission		[6]
$LaLuO_3$	29 850	22 400	7450	[12]

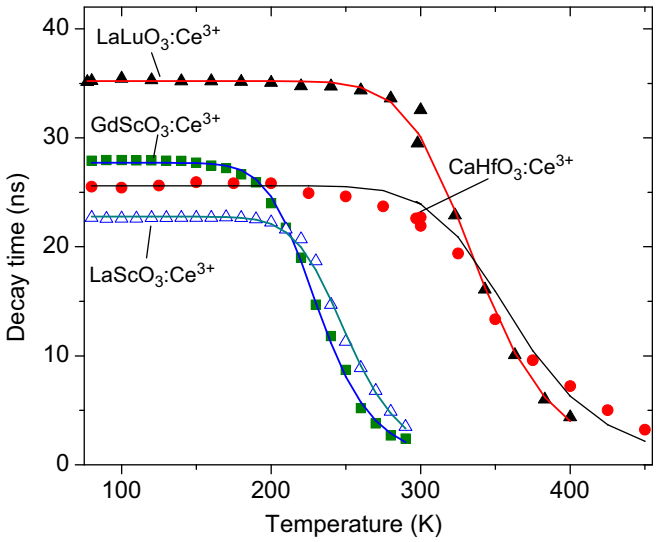

Fig. 2. Decay time versus temperature for $La_{0.999}Ce_{0.001}LuO_3$ (λ_{ex}=320 nm, λ_{em}=440 nm for $T<300$ K; λ_{ex}=355 nm, λ_{em}=460 nm for $T>300$ K), $La_{0.999}Ce_{0.001}ScO_3$ (λ_{ex}=320 nm, λ_{em}=440 nm), $Gd_{0.999}Ce_{0.001}ScO_3$ (λ_{ex}=320 nm, λ_{em}=440 nm) and $Ca_{0.999}Ce_{0.001}HfO_3$ (λ_{ex}=320 nm, λ_{em}=440 nm). The drawn lines are the best least-squares fit to Eq. (1) for the non-radiative rate with a constraint that the attempt frequency, A, is greater than $10^{13}\,s^{-1}$.

Table 2
Activation energies and attempt frequencies for Ce^{3+} $5d^1$ ionization in perovskite hosts.

Host	E_a (eV)	A (s^{-1})	Reference
$CaHfO_3$	0.39	1×10^{13} (fixed)	This work
$LaScO_3$	0.29	3.0×10^{13}	This work
$GdScO_3$	0.26	1.2×10^{13}	This work
$LaLuO_3$	0.39	2.1×10^{13}	This work
$GdAlO_3$	0.29 (PL intensity)	Not reported	[27]
	0.34 (photoconductivity)	1.5×10^{12}	
$LaAlO_3$	<0		[6]

emission quenching and the presence of a slower afterglow component in the decay profile is experimental evidence of photoionization-based quenching since photoionization is the first step for afterglow for excitation energies less than the bandgap [21]. The assignment of Ce^{3+} luminescence quenching by photoionization in $CaHfO_3$ is then similar to other perovskites, such as $GdAlO_3$ [6] and $LaAlO_3$ [7], where Ce^{3+} luminescence quenching has also been assigned to photoionization.

The analysis of the decay time versus temperature (Fig. 2) uses an Arrhenius relationship for the rate of thermal ionization from the Ce^{3+} $5d^1$ level

$$\Gamma_{PI} = A\exp(-E_a/kT) \quad (1)$$

where E_a is the activation energy and A is an attempt frequency. The high temperature ($T>300$ K) afterglow complicates this analysis since afterglow makes the decay profiles non-exponential. We minimized the effect of the afterglow by analyzing the time constant of the initial component (0–50 ns) of the decay profile. Using this procedure, the least-squares fit of A and E_a for the $CaHfO_3:Ce^{3+}$ decay time versus temperature for gives $A=2.9\times10^{11}\,s^{-1}$ and $E_a=0.28$ eV. However, when comparing the values of A and E_a for quenching in $CaHfO_3:Ce^{3+}$ with the other hosts studied in here (*vide infra* and Table 2), this attempt frequency is ~2 orders of magnitude lower for $CaHfO_3:Ce^{3+}$ versus other perovskite hosts that have more typical values of A $\sim10^{13}\,s^{-1}$. When constraining the attempt frequency to be greater than $10^{13}\,s^{-1}$, the least-squares fit gives $E_a=0.39$ eV. Since we have no physical reason for a 2 orders of magnitude lower attempt frequency in $CaHfO_3:Ce^{3+}$, except for an overestimate in the high temperature decay times due to afterglow, we use $E_a=0.39$ eV as the activation energy for Ce^{3+} quenching in $CaHfO_3$ when comparing with other perovskite hosts.

In contrast to $CaHfO_3:Ce^{3+}$, the luminescence from $CaZrO_3:Ce^{3+}$ is almost completely quenched at room temperature. However, $CaZrO_3:Ce^{3+}$ shows a strong absorption band with a maximum at ~335–340 nm (Fig. 3a), similar to the main Ce^{3+} excitation band in $CaHfO_3:Ce^{3+}$ (Fig. 1a). This absorption band in $CaZrO_3:Ce^{3+}$ is assigned to a Ce^{3+} center similar to the main Ce^{3+} center in $CaHfO_3$. The similar energy position for the lowest Ce^{3+} $4f^1\rightarrow5d^1$ transition in $CaZrO_3$ and $CaHfO_3$ is reasonable since $CaZrO_3$ and $CaHfO_3$ are isostructural with similar ionic radii for Zr^{4+} and Hf^{4+} [16]. While there is virtually no emission intensity when exciting the main Ce^{3+} center at ~340 nm, there is a doublet emission band (λ_{max}~550 nm) characteristic of Ce^{3+} emission with excitation bands at ~385 and 420 nm (Stokes shift of ~4000 cm^{-1}) at 10 K (Fig. 3a). While these luminescence excitation bands do not correspond to the main Ce^{3+} absorption band that is measured in diffuse reflectance, the low temperature

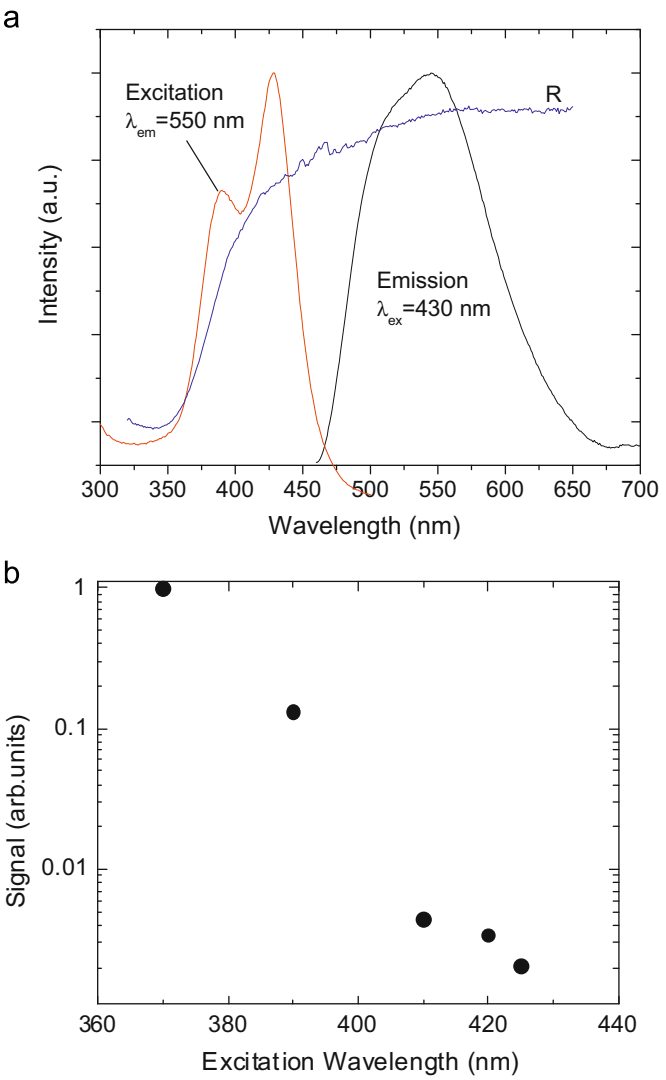

Fig. 3. (a) Emission (λ_{ex}=430 nm) and excitation spectra of (λ_{em}=550 nm) of $Ca_{0.99}Ce_{0.01}ZrO_3$ at ~10 K with the room temperature diffuse reflectance; and (b) Integrated thermoluminescence excitation spectra of $Ca_{0.99}Ce_{0.01}ZrO_3$ (the y-axis has a logarithmic scale).

decay time of this emission is ~40 ns, characteristic of the allowed Ce^{3+} $5d^1 \rightarrow 4f^1$ emission transition. This emission band is assigned to a minority Ce^{3+} center in $CaZrO_3$ that arises from differences in the local charge compensation when Ce^{3+} replaces Ca^{2+} in $CaZrO_3$. This minority site apparently has a higher crystal field splitting and/or centroid shift since the lowest Ce^{3+} $5d^1$ level is at lower energy. There is still strong thermal quenching of this minority Ce^{3+} luminescence with virtually no luminescence intensity at ~200 K. TLES experiments directly indicate that the strong luminescence quenching for majority and minority Ce^{3+} sites in $CaZrO_3$:Ce^{3+} is due to photoionization. The approximate onset of the thermoluminescence (TL) signal at ~435 nm corresponds to the minority Ce^{3+} $4f^1 \rightarrow 5d^1$ excitation band in $CaZrO_3$, and there is stronger TL signal when exciting into the main Ce^{3+} center in $CaZrO_3$ (Fig. 3b). Therefore, mobile charge carriers are formed when majority and minority Ce^{3+} sites are excited at ~80 K, indicating that the two main Ce^{3+} centers in $CaZrO_3$ ionize under $4f^1 \rightarrow 5d^1$ excitation. Presumably, most (but not all) of the electrons in the conduction band reach quenching sites before recombining with Ce^{4+} ions that are created by optical excitation and photoionization.

3.2. Luminescence of $LaScO_3$:Ce^{3+} and $GdScO_3$:Ce^{3+}

The position of the Ce^{3+} emission and excitation bands in $LaScO_3$:Ce^{3+} and $GdScO_3$:Ce^{3+} are also at lower energies versus the Al^{3+} perovskites with larger Stokes shifts (Fig. 4 and Table 1). The Ce^{3+} excitation spectrum in $GdScO_3$:Ce^{3+} has the Gd^{3+} $^8S_{7/2} \rightarrow {}^6I_J$ absorption transition (Fig. 4b), evidence of $Gd^{3+} \rightarrow Ce^{3+}$ energy transfer from the spectral overlap between Gd^{3+} $^6P_J \rightarrow {}^8S_{7/2}$ emission and Ce^{3+} $4f^1 \rightarrow 5d^1$ absorption transitions. Since we cannot determine the energy position of each Ce^{3+} $5d^1$ level in the Sc^{3+} perovskites, changes in the Ce^{3+} $5d^1$ centroid shift, ε_c, are quantified using the average cation electronegativity combined with RE^{3+}–O^{2-} bond lengths [2,17]

$$\varepsilon_c = 1.79 \times 10^{13} \sum_{i=1}^{N} \frac{\alpha_{sp}^i}{(R_i - 0.6\Delta R)^6} \quad (2)$$

$$\alpha_{sp} = 0.33 + \frac{4.8}{\chi_{av}^2} \quad (3)$$

where R_i is the RE^{3+}-anion distance, N is the number of anions coordinated to Ce^{3+}, ΔR is the difference in ionic radii for RE^{3+} and Ce^{3+}, and χ_{av} is the weighted average of the cation electronegativity. Using the crystallographic data for $LaScO_3$ [18], $GdScO_3$ [18], and $LaAlO_3$ [19], the calculated Ce^{3+} $5d^1$ centroid shifts are 15 950, 15 750, and 14 500 cm^{-1}, respectively. The difference in the estimated Ce^{3+} $5d^1$ centroid shift between $LaScO_3$ and $LaAlO_3$ is close to the energy difference between the lowest energy Ce^{3+} $4f^1 \rightarrow 5d^1$ transition in these hosts (Table 1). Therefore, it is likely that the Ce^{3+} $5d^1$ crystal field splitting is similar for $LaScO_3$ and $LaAlO_3$. Within perovskite hosts, the Ce^{3+} $5d^1$ crystal field splitting is dependent upon both the Ce^{3+}–O^{2-} bond length and the distortion from the ideal 12-coordinated A-site in cubic perovskites [1]. Typically, this A-site distortion is larger when the A and B-site perovskite cations are closer in size. Therefore, the larger A-site distortion in $LaScO_3$ versus $LaAlO_3$ may compensate for the longer bond length in $LaScO_3$ [18], giving a similar Ce^{3+} $5d^1$ crystal field splitting in $LaAlO_3$ and $LaScO_3$. However, for $GdScO_3$, the smaller Gd^{3+}–O^{2-} bond length [18] and the larger A-site distortion should lead to a larger crystal field splitting [1] versus both $LaScO_3$ and $LaAlO_3$, explaining the lower energy for the lowest energy Ce^{3+} $4f^1 \rightarrow 5d^1$ transition.

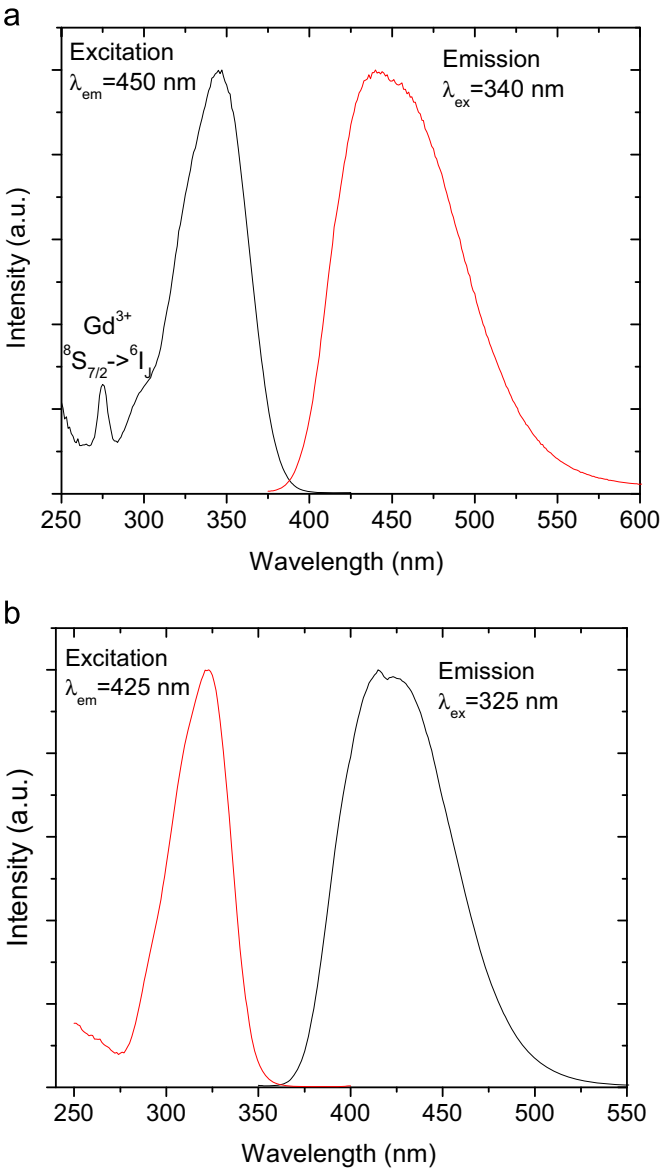

Fig. 4. (a) Emission (λ_{ex}=340 nm) and excitation spectra of (λ_{em}=450 nm) of $Gd_{0.999}Ce_{0.001}ScO_3$ at ~10 K; and (b) Emission (λ_{ex}=325 nm) and excitation spectra of (λ_{em}=425 nm) of $La_{0.999}Ce_{0.001}ScO_3$ at ~10 K.

Comparing the Sc^{3+} perovskites with the Hf^{4+}/Zr^{4+} perovskites, the estimated centroid shift in the Sc^{3+} perovskites is ~1000 cm^{-1} smaller (ε_c~16700 cm^{-1} in $CaZrO_3$), due to the larger average cation electronegativity. Therefore, a lower energy Ce^{3+} $5d^1$ centroid can explain the relative energy differences between the lowest Ce^{3+} $4f^1 \rightarrow 5d^1$ transition in $LaScO_3$ and $CaHfO_3$ (Table 1) since La^{3+}/Sc^{3+} and Ca^{2+}/Hf^{4+} have similar ionic radii [16]. However, differences in the $5d^1$ centroid cannot account for the trend between $CaHfO_3$ and $GdScO_3$. When comparing $CaHfO_3$ and $GdScO_3$, the lower energy of the lowest Ce^{3+} $4f^1 \rightarrow 5d^1$ transition in $GdScO_3$ is likely due to a stronger crystal field splitting of the Ce^{3+} $5d^1$ levels, from the smaller ionic radii of Gd^{3+} [16] and the larger A-site distortion in $GdScO_3$.

While the position of the Ce^{3+} emission and excitation bands in the Sc^{3+} perovskites is not unusual compared to other perovskites (Table 1), the Ce^{3+} emission in $LaScO_3$ and $GdScO_3$ is strongly quenched at room temperature unlike $CaHfO_3$:Ce^{3+} and $LaLuO_3$:Ce^{3+} (Fig. 2). The Ce^{3+} concentration in these Sc^{3+} perovskites is ~0.1%, and the spectral overlap between the

Ce^{3+} $4f^1 \rightarrow 5d^1$ absorption and Ce^{3+} $5d^1 \rightarrow 4f^1$ emission is small (Fig. 4). Therefore, energy migration and concentration quenching should be minimal in the thermal quenching of Ce^{3+} luminescence, making it intrinsic in nature.

The two main causes for intrinsic, thermally activated non-radiative transitions from the Ce^{3+} $5d^1$ are ionization or level crossing between the lowest energy $5d^1$ level and the $4f^1$ levels. In the Sc^{3+} perovskites, the thermal quenching is assigned to Ce^{3+} $5d^1$ ionization as in $LaAlO_3$ [6], $GdAlO_3$ [7], and Ca(Hf,Zr)O_3 and not due to level crossing. First, if level crossing is the primary quenching mechanism, the position of the lowest Ce^{3+} $5d^1$ level and the Stokes shift should be indicators for the quenching temperature [20]. Comparing the energy positions of the lowest Ce^{3+} $5d^1$ level and the Stokes shift in $LaScO_3$, $GdScO_3$, $CaHfO_3$, and $LaLuO_3$ (Table 1), there is no correlation between these factors and the quenching of Ce^{3+} $5d^1 \rightarrow 4f^1$ emission. For example, $LaLuO_3$:Ce^{3+} and $LaScO_3$:Ce^{3+} have similar Stokes shifts but the energy position of the lowest Ce^{3+} $5d^1$ level is much lower in $LaLuO_3$. If level crossing is the primary quenching mechanism, $LaLuO_3$:Ce^{3+} should have a much stronger thermal quenching versus $LaScO_3$:Ce^{3+}; this is directly opposite to these experimental observations (Fig. 2). In addition, as the initial decay time of $LaScO_3$:Ce^{3+} and $GdScO_3$:Ce^{3+} decreases, the decay profile deviates from a single exponential with an additional weak component (intensity is $<10\%$ of the main Ce^{3+} decay component) that has a decay time of >50 ns (Fig. 5). Similar to $CaHfO_3$:Ce^{3+}, this slower decay component is assigned to an afterglow luminescence that occurs after charge carriers are created, trapped at defects, and slowly detrapped from those defects. Again, the correlation between afterglow and a reduction in decay time is evidence for Ce^{3+} luminescence quenching by photoionization.

The activation energy for thermal ionization from the lowest Ce^{3+} $5d^1$ level is estimated using the decay times for the initial fast component of the Ce^{3+} decay profile of $LaScO_3$, $GdScO_3$, and $LaLuO_3$ using Eq. (1) for thermal ionization rate, Γ_{PI} (Table 2). The least-squares fit of the decay time versus temperature gives $A=3.0\times10^{13}\,s^{-1}$ and $E_a=0.29$ eV for $LaScO_3$; $A=1.2\times10^{13}\,s^{-1}$ and $E_a=0.26$ eV for $GdScO_3$; and $A=2.1\times10^{13}\,s^{-1}$ and $E_a=0.39$ eV for $LaLuO_3$ (Fig. 3a). These activation energies are comparable to the activation energy for luminescence quenching and photoconductivity in $GdAlO_3$, ~0.3 eV [7] but are much smaller than the activation energy for luminescence quenching in $YAlO_3$, 1.2 eV [22].

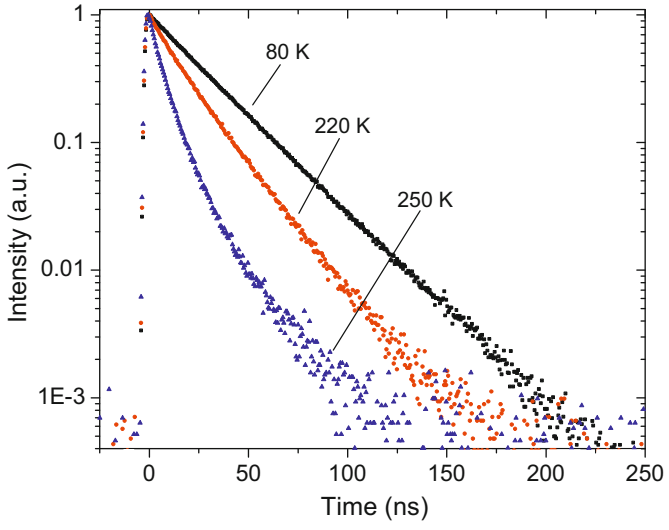

Fig. 5. Decay profile for $Gd_{0.999}Ce_{0.001}ScO_3$ ($\lambda_{ex}=320$ nm, $\lambda_{em}=440$ nm) versus temperature. The background has been subtracted from these decay profiles.

3.3. Comparison of Ce^{3+} $5d^1$ ionization in perovskite hosts

From these experiments, thermally activated ionization is the main Ce^{3+} $5d^1 \rightarrow 4f^1$ luminescence quenching mechanism in the nd^0 perovskites, similar to the aluminate perovskites [6,7]. The key parameter for thermally activated ionization is the energy difference between the lowest Ce^{3+} $5d^1$ level and the host conduction band. This section discusses how this parameter is affected in the orthorhombic perovskites through the host bandgap, the position of the Ce^{3+} $4f^1$ ground state within the bandgap, and the position of the lowest energy $4f^1 \rightarrow 5d^1$ transition. These parameters are connected using a Born–Haber relationship to estimate photoionization thresholds [10]

$$E_g = E_{PI}(Ce^{3+}) + E_{CTB}(Ce^{4+}-O^{2-}) \quad (4)$$

where E_g is the host lattice bandgap, $E_{PI}(Ce^{3+})$ is the Ce^{3+} photoionization threshold from the $4f^1$ ground state, and $E_{CTB}(Ce^{4+}-O^{2-})$ is the energy for the Ce^{4+}–O^{2-} charge transfer band (CTB). The photoionization barrier from the lowest energy Ce^{3+} $5d^1$ level is then the energy of the lowest $4f^1 \rightarrow 5d^1$ transition subtracted from $E_{PI}(Ce^{3+})$.

Within this analysis, the charge compensation for main Ce^{3+} center in $CaHfO_3$ and $CaZrO_3$ is assumed to be distant. This assumption is supported by the correlation of the position of the lowest Ce^{3+} $5d^1$ level to the estimated Ce^{3+} $5d^1$ centroid shift and the Stokes shift for Ce^{3+} luminescence in $CaHfO_3$; local charge compensation would strongly affect the position of the lowest Ce^{3+} $5d^1$ level and the Stokes shift. However, this is a tentative assumption, and local charge compensation in the Hf^{4+} and Zr^{4+} perovskites could affect the position of the Ce^{3+} $4f^1$ ground state in the host bandgap [23]. In addition, as discussed in detail in Section 3.1, the estimate of E_a for $CaHfO_3$:Ce^{3+} is problematic. Therefore, it is important to note that this discussion is primarily qualitative.

The most straightforward comparison within these perovskites is between the main Ce^{3+} centers in $CaZrO_3$ and $CaHfO_3$. The coordination of the main Ce^{3+} center is very similar in these perovskites as shown by the similar energy for the lowest energy Ce^{3+} $4f^1 \rightarrow 5d^1$ transition. Given the similar size and electronegativity for Hf^{4+} and Zr^{4+} [15,16], the energy position of the $4f^1$ Ce^{3+} ground state versus the valence band should be similar for the main Ce^{3+} center in $CaZrO_3$ and $CaHfO_3$. Therefore, the main difference between the main Ce^{3+} centers in $CaZrO_3$ and $CaHfO_3$ is that the relative energy position of Ce^{3+} $5d^1$ level versus the host conduction band is lower by ~0.5 eV due to a smaller $CaZrO_3$ bandgap. This difference leads to total quenching of the main center Ce^{3+} luminescence in $CaZrO_3$ in comparison to $CaHfO_3$:Ce^{3+} where the onset for thermal quenching is ~270 K. It is more difficult to make comparisons with the secondary Ce^{3+} center in $CaZrO_3$ (Fig. 3a) since the local coordination is not known. In a qualitative sense, however, the lower energy position of lowest $5d^1$ level for the minority Ce^{3+} center in $CaZrO_3$ should increase the activation barrier for ionization as observed in the higher quenching temperature for this minority Ce^{3+} center in $CaZrO_3$.

It is also possible to use Eq. (4) when analyzing Ce^{3+} photoionization quenching in more complicated situations versus the relatively simple comparison between $CaHfO_3$:Ce^{3+} and $CaZrO_3$:Ce^{3+}. For example, $CaHfO_3$ and the Sc^{3+} perovskites have similar values for the host lattice absorption edge [8,9] and the lowest energy Ce^{3+} $4f^1 \rightarrow 5d^1$ transition (Table 1). However, the larger E_{PI} in $CaHfO_3$ can be explained by an effective positive charge when Ce^{3+} replaces Ca^{2+}. An effective positive charge typically lowers the energy of metal-ligand charge transfer bands [24], leading to a larger E_{PI} when using Eq. (4). Taking the thermal

activation energies for Ce^{3+} photoionization in the Sc^{3+} perovskites, the shift in the energy position of the Ce^{3+} $4f^1$ ground state versus the valence band between $CaHfO_3$ and the Sc^{3+} perovskites is estimated to be at least 0.1 eV. In addition, the difference in the activation energy for luminescence quenching between $LaScO_3$:Ce^{3+} and $LaLuO_3$:Ce^{3+} is similar to the difference in the energy position of the lowest $4f^1 \rightarrow 5d^1$ transition (Table 1). Using Eq. (4), the relative position of the Ce^{3+} $4f^1$ ground state versus the host conduction band should then be similar for $LaScO_3$ and $LaLuO_3$. When comparing the scandate hosts, the lower energy position of the $5d^1$ levels in $GdScO_3$:Ce^{3+} should increase the photoionization energy barrier in $GdScO_3$:Ce^{3+} versus $LaScO_3$:Ce^{3+}. However, the shorter Gd^{3+}–O^{2-} bond lengths in $GdScO_3$ will also increase $E_{CTB}(Ce^{4+}–O^{2-})$ [25]. It appears that the higher CTB energy counteracts the lower $5d^1$ energy since the activation energy for Ce^{3+} luminescence quenching are similar for $LaScO_3$:Ce^{3+} and $GdScO_3$:Ce^{3+} (Fig. 2 and Table 2). Since this is mainly a qualitative analysis, further measurements and analysis are required to determine the accuracy of these estimates using the relationship in Eq. (4).

Finally, we briefly compare the Ce^{3+} quenching in these nd^0 perovskites to the Al^{3+} perovskites. For example, the position of the lowest energy Ce^{3+} $4f^1 \rightarrow 5d^1$ transition of $LaScO_3$ and $LaAlO_3$ is similar (Table 1) as is the fundamental absorption edge [6,9]. However, Ce^{3+} luminescence is completely quenched in $LaAlO_3$ at all temperatures [6]. While there are experimental uncertainties in the exact value of the host bandgap, the relative position of the Ce^{3+} $4f^1$ ground state in the bandgap can explain the differences between $LaScO_3$ and $LaAlO_3$. Since Al^{3+} is smaller than Sc^{3+} and the average La^{3+}–O^{2-} bond length is smaller in $LaAlO_3$ [19] versus $LaScO_3$ [18], $E_{CTB}(Ce^{4+}–O^{2-})$ should be at a higher energy in $LaAlO_3$ [25]. This should lead to a smaller $E_{PI}(Ce^{3+})$ for $LaAlO_3$ (Eq. (4)), correlating to the basic Ce^{3+} luminescence quenching trends. The position of the Ce^{3+} ground state with respect to the valence band is at least $\sim$0.3 eV higher in $LaAlO_3$ versus $LaScO_3$ based upon the total quenching of Ce^{3+} luminescence in $LaAlO_3$.

4. Conclusions

In this report, Ce^{3+} luminescence in several perovskite hosts has been described and compared. When comparing the Ce^{3+} luminescence in these hosts to that in the Al^{3+} perovskites, we find that the lower electronegativity of the B-site cations leads to a larger Ce^{3+} $5d^1$ centroid shift, generally lowering the energy position for the lowest energy Ce^{3+} $4f^1 \rightarrow 5d^1$ absorption transition. In addition, we find a larger Stokes shift in these Hf^{4+}/Zr^{4+}/Sc^{3+} perovskites versus the Al^{3+} perovskites. Finally, we show that non-radiative transitions in these materials are due to photoionization, as in the Al^{3+} perovskites. However, in spite of the nd^0 electronic configuration of the B-site cations giving relatively low energy bandgaps, the extent of Ce^{3+} photoionization quenching is comparable to many of the Al^{3+} perovskites. The differences in photoionization can be qualitatively correlated to the relative energy position of the lowest energy Ce^{3+} $5d^1$ level versus the host conduction band and the composition of these perovskites. Additional analysis and experiments could quantify these comparisons and accurately place the energy position of the Ce^{3+} $4f^1$ ground state within the bandgap of these perovskites.

Acknowledgments

This presented in this report was partially supported by the US Department of Energy through contract# DE-FC26-06NT42934. This report was prepared as an account of work sponsored by an agency of the United States Government. Neither the United States Government nor any agency thereof, nor any of their employees, makes any warranty, express or implied, or assumes any legal liability or responsibility for the accuracy, completeness, or usefulness of any information, apparatus, product, or process disclosed, or represents that its use would not infringe privately owned rights. Reference herein to any specific commercial product, process, or service by trade name, trademark, manufacturer, or otherwise does not necessarily constitute or imply its endorsement, recommendation, or favoring by the United States Government or any agency thereof. The views and opinions of authors expressed herein do not necessarily state or reflect those of the United States Government or any agency thereof.

References

[1] P. Dorenbos, J. Lumin. 99 (2002) 283–299.
[2] P. Dorenbos, Phys. Rev. B 65 (2002) 235110.
[3] G. Blasse, W. Schipper, J.J. Hamelink, Inorg. Chim. Acta 189 (1991) 77–80.
[4] P. Dorenbos, J. Phys.: Condens. Matter 15 (2003) 8417–8434.
[5] S.H.M. Poort, W.P. Blokpoel, G. Blasse, Chem. Mater. 7 (1995) 1547–1551.
[6] E. van der Kolk, J.T.M. de Haas, A.J.J. Bos, C.W.E. van Eijk, P. Dorenbos, J. Appl. Phys. 101 (2007) 083703.
[7] E. van der Kolk, P. Dorenbos, J.T.M. de Haas, C.W.E. van Eijk, Phys. Rev. B 71 (2005) 045121.
[8] W.J. Schipper, J.J. Piet, H.J. De Jager, G. Blasse, Mater. Res. Bull. 29 (1994) 23–30.
[9] G. Lucovsky, J.G. Hong, C.C. Fulton, Y. Zou, R.J. Nemanich, H. Ade, D.G. Scholm, J.L. Freeouf, Phys. Status Solidi (b) 241 (2004) 2221–2235.
[10] W.C. Wong, D.S. McClure, S.A. Basun, M.R. Kokta, Phys. Rev. B 51 (1995) 5682–5692.
[11] J. Fleniken, J. Wang, J. Grimm, M.J. Weber, U. Happek, J. Lumin. 94-95 (2001) 465–469.
[12] P. Dorenbos, J. Lumin. 91 (2000) 155–176.
[13] W. Jia, D. Jia, T. Rodriguez, Y. Wang, H. Kiang, K. Li, J. Lumin. 122–123 (2007) 55–57.
[14] L. Zhang, C. Madej, C. Pédrini, B. Moine, C. Dujardin, A. Petrosyan, A.N. Belsky, Chem. Phys. Lett. 268 (1997) 408–412.
[15] L. Pauling, The Nature of the Chemical Bond, Cornell University Press, 1960.
[16] R.D. Shannon, C.T. Prewitt, Acta Crystallogr. B 25 (1969) 925–946; R.D. Shannon, C.T. Prewitt, Acta Crystallogr. B 26 (1970) 1046–1048.
[17] P. Dorenbos, J. Lumin. 105 (2003) 117–119.
[18] R.P. Liferovich, R.H. Mitchell, J. Solid State Chem. 177 (2004) 2188–2197.
[19] S. Geller, V.P. Bala, Acta Crystallogr. 9 (1956) 1019–1025.
[20] K.C. Bleijenberg, G. Blasse, J. Sol. State Chem. 28 (1979) 303–307.
[21] A.A. Setlur, A.M. Srivastava, H.L. Pham, M.E. Hannah, U. Happek, J. Appl. Phys. 103 (2008) 053513.
[22] L.-J. Lyu, D.S. Hamilton, J. Lumin. 48–49 (1991) 251–254.
[23] S.A. Basun, S.P. Feofilov, A.A. Kaplyanskii, U. Happek, J. Choi, K.W. Jang, R.S. Meltzer, Phys. Rev. B 61 (2000) 12848–12853.
[24] J. Alarcon, D. van der Voort, G. Blasse, Mater. Res. Bull. 27 (1992) 467–472.
[25] G. Blasse, A. Bril, Philips Tech. Rev. 31 (1970) 304–334.
[26] M.J. Weber, J. Appl. Phys. 44 (1973) 3205–3208.
[27] J. Fava, G. Le Flem, J.C. Bourcet, F. Gaume-Mahn, Mater. Res. Bull. 11 (1976) 1–9.